Supporting Information for

"State-of-the-art local correlation methods enable affordable gold standard quantum chemistry up to hundreds of atoms"

Péter R. Nagy[*,†,‡,¶]

† *Department of Physical Chemistry and Materials Science, Faculty of Chemical Technology and Biotechnology, Budapest University of Technology and Economics, Műegyetem rkp. 3., H-1111 Budapest, Hungary*

‡ *HUN-REN-BME Quantum Chemistry Research Group, Műegyetem rkp. 3., H-1111 Budapest, Hungary*

¶ *MTA-BME Lendület Quantum Chemistry Research Group, Műegyetem rkp. 3., H-1111 Budapest, Hungary*

E-mail: nagy.peter@vbk.bme.hu

S1 Further details of local correlation approaches

We note in Sect. 2 of the main text, that the invariance of the correlation energy to unitary orbital transformations is exploited when working in the LMO basis. However, the equations for the perturbative methods become coupled in such non-canonical basis sets. This coupling introduces a smaller difficulty at the MP2 level, but it is more complex to handle efficiently, e.g., for the (T) correction of CCSD(T) with the coupled or direct methods. However, the use of the LMO basis is still worthwhile as they provide faster decay for the wave function parameters with distance. To that end, often a hierarchy of distant, weak, strong, etc. LMO pair lists is introduced, whose interaction is computed with methods of increasing accuracy and cost. Such methods can be combined with orbital- or orbital-pair specific NO approximations, leading to LNOs (or similar OSVs[1]) and PNOs. They efficiently compress the wave function expansion in the unoccupied MO space due to their focused role of correlating electrons only of a specific LMO or LMO pair. The drawback is the separate set of orbitals (and corresponding ERIs) for each LMO or LMO pair. Thus, especially for the latter combined with coupled methodologies, transforming the ERIs to all the different pair-specific NO basis requires a large amount of operations and intermediate data that has to be accessible for the whole molecule during the entire CC computation.

Additional similarities and differences between LNO and PNO methods can also be noted. For example, the unoccupied LNOs are computed for each LMO form a density matrix that collects contributions from all strong pairs of that LMO. Thus, the virtual LNOs can also be interpreted as a weighted average of PNOs corresponding to a specific LMO and all of its strongly interacting LMO pairs.[2] Consequently, the number of LNOs per LMO is usually larger than that of PNOs determined for a single LMO pair. However, there is a different LNO basis set for each LMO and a different PNO basis set for each (non-distant) LMO pair. Thus, the total number of different PNOs for the entire molecule is usually larger than that of the total number of LNOs. Moreover, the LNO method enables the LNO compression of the occupied domain space, while other methods work in the uncompressed occupied LMO

space.

S2 Further details of the LNO method and algorithm

The steps of a practical LNO computation (Figure S1) begin with computing the HF or Kohn–Sham (KS) orbitals for the entire molecule and the localization of the occupied orbitals (except for the core orbitals left out from the correlated treatment). Next, we provide additional technical details expanding on the introduction in Sects. 2.2–2.3 of the main text.
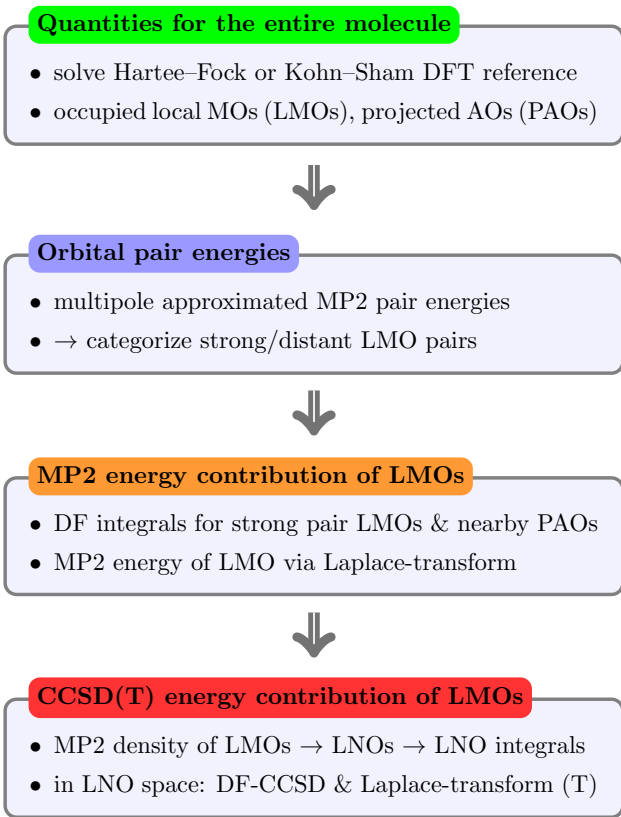
Quantities for the entire molecule
- solve Hartee–Fock or Kohn–Sham DFT reference
- occupied local MOs (LMOs), projected AOs (PAOs)

⇓

Orbital pair energies
- multipole approximated MP2 pair energies
- → categorize strong/distant LMO pairs

⇓

MP2 energy contribution of LMOs
- DF integrals for strong pair LMOs & nearby PAOs
- MP2 energy of LMO via Laplace-transform

⇓

CCSD(T) energy contribution of LMOs
- MP2 density of LMOs → LNOs → LNO integrals
- in LNO space: DF-CCSD & Laplace-transform (T)

Figure S1: Main algorithmic steps of the LNO-CCSD(T) method.

To obtain the orbital pair energies ($\delta E_{IJ}^{\mathrm{MP2}}$), several methods,[3–5] including our LNO approach, employ fast multipole approximations for the energy contribution of distant pairs below 10^{-5}–10^{-6} hartree pair energies or about 10^{-3}–$10^{-5}\%$ of the correlation energy. The strict control of the distant LMO pair list and higher-order multipole contributions up to octupoles allow in the LNO methods to suppress this source of correlation energy error to

3

around a hundredth of a percent for the entire molecule,[2,6] while keeping an asymptotically linear-scaling and manageable number of strongly interacting LMO pairs.

While for a molecule of a few (one) hundred atoms only about a few (few ten) percent of the LMO pairs are strongly interacting, this amount of orbitals/electrons prohibits the use of conventional correlation methods (besides MP2) to obtain the M1 level correlation energy contributions for large molecules. Thus, in a domain built for the strong pairs of each LMO, we compute the M2 level (currently MP2) estimate of the final, M1 level [e.g., CCSD(T)] wave function. The so-obtained M2 (e.g., first-order MP) amplitudes are used to construct LMO-specific density matrices to determine the occupied and virtual LNO bases (i.e., the summation restriction and bases employed in Eq. 2 of the main text) and the domain correlation energies [δE_I^{M2} of Eq. 3 at the MP2 level]. Then, the M1-level correlation energies are computed in the LNO bases compressed according to the complexity of the M2-level wave function probe.

Here, local correlation methods face a technical complication, namely that the ratio of the number of virtual over occupied LNOs is relatively small compared to the canonical case without local and/or NO approximations. Therefore, we developed and optimized novel CCSD and (T) algorithms, especially to handle small virtual over occupied orbital number ratios.[7,8] Moreover, the size of the occupied and virtual LNO bases can still be considerable for complicated molecules. To handle large orbital spaces, our conventional CCSD and (T) codes have outstanding peak-performance utilization as well as memory- and disk-economic design due to exploiting all permutational symmetries and a DF-based integral-direct algorithm optimization for all terms.[7,8] These algorithms are also generalized and employed for the domain CCSD(T) computations in the LNO basis. Additionally, all terms of the CCSD and (T) parts are optimized including those which only become relatively costly for small virtual over occupied orbital dimensions. We have also devoted considerable optimization efforts to decrease the data demand of the LNO methods by introducing integral-direct local integral transformation, MP2 and CCSD(T) algorithms.[2,5,6]

Regarding the open-shell case, obtaining the reference determinant could be more complicated. Therefore ROHF and ROKS, as well as UHF, UKS, and corresponding quasi-restricted[9] reference orbitals are also implemented.[10,11] If needed, all these references are converted to an RO formalism as the cost of integral transformation becomes similar to that of the closed-shell case. Additionally, utilizing our unique long-range spin polarization approximation, we can reuse the more economical closed-shell LNO-CCSD(T) codes for the domains which are not interacting strongly with any singly-occupied LMOs.[10,11]

It is also worth noting that our LMP2 correlation energy is obtained with the same domain and pair approximations as LNO-CCSD(T), but NO approximations are not introduced for LMP2. Therefore, the LMP2 correlation energy

$$E^{\text{LMP2}} = \sum_I \left[\delta E_I^{\text{MP2}} + \frac{1}{2} \sum_J^{\text{distant p.}} \delta E_{IJ}^{\text{MP2}} \right], \tag{S1}$$

is also obtained without additional cost in all LNO-CCSD(T) computations.

S3 Similarity of the LAF and CPS extrapolations for the LNO and PNO methods

This LAF extrapolation expression in Eq. 5 of the main text can be reformulated as

$$E_{\text{LAF}}^{\text{S}-(\text{S}+1)} = E^{\text{S}} + \text{F}(E^{\text{S}+1} - E^{\text{S}}) \pm 0.5(E^{\text{S}+1} - E^{\text{S}}), \tag{S2}$$

where we subtracted $(E^{\text{S}+1} - E^{\text{S}})$ from the first term of Eq. 5 and added it to its second term, leading to $F = 1.5$.

The benefit of this rearrangement is that one can point out the similarity of our LAF extrapolation for the LNO methods to the recently proposed complete PNO space (CPS)

extrapolation of Bistoni et al.[12] in the context of DLPNO methods:

$$E_{\mathrm{CPS}}^{\mathrm{X-(X+1)}} = E^{\mathrm{X}} + \mathrm{F}(E^{\mathrm{X+1}} - E^{\mathrm{X}}), \tag{S3}$$

where X labels the employed $10^{-\mathrm{X}}$ PNO truncation threshold. For example, the common CPS(6,7) extrapolation employs the *NormalPNO* and *TightPNO*, that is $X = 6$ and $X+1 = 7$, settings for the CPS extrapolation. The LAF and the CPS extrapolations are similar in the sense that both employ $F = 1.5$ to scale the step size (cf. Eqs. S2 and S3) added to the less converged $E^{\mathrm{S}}/E^{\mathrm{X}}$ value. While the LAF extrapolations employ the *Loose, Normal, Tight*, etc. LNO threshold series without any modification, the CPS extrapolation sets *TightPNO* settings for all approximations other than the PNO truncation for the E^{X} DLPNO computations. Thus, the CPS method extrapolates only the PNO truncation error and does not affect the other DLPNO-based local approximations, which are assumed to be appropriate at the *TightPNO* level. In addition, Martin and co-workers also experimented with optimizing the $F = 1.5$ factor of the LAF extrapolation system specifically. Indeed, this improved the performance of the LAF approach when better F factors could be obtained from the known canonical CCSD(T) correlation energies.[13,14] However, it still needs to be determined how to obtain in practice an improved F factor system specifically without knowing the canonical correlation energy.

S4 Practical tools for accuracy improvement

The LAF extrapolation illustrated in Fig S2 and will be further studied on specific examples in Sect. S7. The general form of the composite energy correction in Eq. 6 of the main text can be formulated as

$$E_{\mathrm{HL,LL}}^{\mathrm{CBS(Y,Z),X}} = E_{\mathrm{HL}}^{\mathrm{X}} + E_{\mathrm{LL}}^{\mathrm{CBS(Y,Z)}} - E_{\mathrm{LL}}^{\mathrm{X}} = E_{\mathrm{HL}}^{\mathrm{X}} + \Delta E_{\mathrm{LL}}^{\mathrm{CBS(Y,Z),X}}, \tag{S4}$$
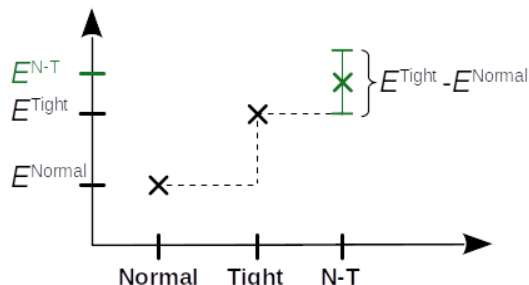
Figure S2: Illustration of the LAF extrapolation of Eq. 4 of the main text yielding the Normal–Tight (N-T) result and uncertainty estimate obtained from the *Normal* and *Tight* LNO-CCSD(T) values.

where X, Y, Z refers to the basis set cardinal numbers. Naturally, such a composite approach can also be interpreted as a HL-LL correction added to the LL/CBS result.

We note that since the performance of MP2 can significantly deteriorate for large molecules, better LL approaches (such as linearized CCSD) have also been suggested in the local correlation context.[15] In general, the composite scheme of Eq. S4 can be extended using various levels of local correlation treatment as follows:

$$E^{\text{CBS}(Y,Z),X}_{\text{HL,LL local CCSD(T)}} = E^{X}_{\text{HL local CCSD(T)}} + \Delta E^{\text{CBS}(Y,Z),X}_{\text{LL local CCSD(T)}}. \tag{S5}$$

Here, the local correlation method can be DLPNO, LNO, or other approaches with an established local approximation hierarchy and the HL (LL) settings can be, e.g., tight (default) local CCSD(T) settings.

Besides the robust $\Delta E^{\text{CBS(T,Q),T}}_{\text{N-T LNO-CCSD(T)}}$ variant, if the type of the application allows, one can consider even more efficient combinations, such as:

$$E^{\text{CBS}(X,X+1),X}_{\text{S LNO-CCSD(T), LMP2}} = E^{X}_{\text{S LNO-CCSD(T)}} + \Delta E^{\text{CBS}(X,X+1),X}_{\text{S LMP2}}, \tag{S6}$$

where S denotes the LNO approximation level (e.g,. *Normal* or N–T). Here, the benefit is that the LMP2/X-ζ result is obtained free as the side product of LNO-CCSD(T)/X-ζ,

while LMP2/$(X+1)$-ζ costs about the same as LNO-CCSD(T)/X-ζ. While not always as reliable as $E_{\text{N-T LNO-CCSD(T)}}^{\text{CBS(T,Q),T}}$, one may try to reduce the computational expense by using $E_{\text{S LNO-CCSD(T)}}^{\text{CBS(T,Q),T}}$ or $E_{\text{S LNO-CCSD(T), LMP2}}^{\text{CBS(T,Q),T}}$ with $S=Normal$ or L–N. Especially in combination with BSSE corrections, it is also worth checking if $\Delta E_{\text{S LNO-CCSD(T)}}^{\text{CBS(D,T),D}}$ type basis set corrections offer a good accuracy over cost performance.

Regarding the uncertainty estimates for the basis set incompleteness error (BSIE), approaches useful for both conventional and local methods can be considered. For example, the size of the $\Delta E_{\text{S LNO-CCSD(T)}}^{\text{CBS(X,X+1),X}}$ or $\Delta E_{\text{S LMP2}}^{\text{CBS(X,X+1),X}}$ basis set corrections are usually a not very tight upper estimate of the remaining BSIE. When available, the difference of the BSSE corrected and uncorrected results and/or the difference of CBS(X,X+1) and CBS(X+1,X+2) results (with X=D or T) offer a more practical and tighter estimate for the BSIE.[16] For the combined uncertainty of the local and BSI errors, the most conservative solution is to sum their absolute values,[16] as currently the distribution of these uncertainties is relatively unknown. Adding together the local and BSI error bars is probably often an overestimation, for example, these sources of error can partly cancel (see, e.g., Figs. 5–7 and S4–S9). Thus, some authors prefer to take their root sum square.[17]

Considering these ideas, for example, for the specific example of the halocyclization reaction of Fig. 6, the *veryTight* LNO-CCSD(T) computations at the Q-ζ or 5-ζ level would be long but feasible due to their accessible memory demand and restartability. However, observing the almost parallel LNO convergence with all basis set levels motivates the application of a composite approach (see also in Sect. 3.4 of the main text). Namely, e.g., the well converged LNO-CCSD(T) results at the aug-cc-pVTZ basis set can be accurately combined with a basis set correction obtained at the *Tight*, N–T, or often even at the *Normal* LNO-CCSD(T)/CBS(T,Q) level, if one verifies that the target accuracy is reached on a representative example. Convincingly, the *NormalPNO* DLPNO-CCSD(T$_1$)/CBS(T,Q) level basis set correction with respect to the DLPNO-CCSD(T$_1$)/aug-cc-pVTZ barrier height agrees well with the corresponding correction obtained with the LNO-CCSD(T) method.

S5 Additional benchmarks

Table S1: Summary of local CCSD(T) benchmarks in the literature for various energy difference properties extending Table 4 of the main text with additional details. Mean absolute error (MAE) and maximum error [in kcal/mol] against canonical CCSD(T) for the LNO-CCSD(T) and DLPNO-CCSD(T_1) methods are collected in the last columns corresponding to their default or tight (italicized) settings. Results in rows labeled with † symbols were evaluated independently from LNO and DLPNO method developers.

test set	process	entries	No. of atoms AVG	No. of atoms MAX	basis set	thresholds	DLPNO error MAE	DLPNO error MAX	LNO error MAE	LNO error MAX
organic[18]	atomization[a]	31	7.9	14	aug-cc-pVQZ	*tight*	*0.64*[18]	*2.15*	*0.40*[18]	*0.79*[†]
RSE30[19]	radical reactions	30	9.3	13	aug-cc-pVTZ	default	0.17[20]	0.47	0.04[11]	0.11
IP21[10]	ionization	21	9.8	17	aug-cc-pVTZ	default	0.72[20]	3.25	0.16[11]	0.62
NWH[21]	reactions	23	13.5	36	cc-pVTZ	default	0.31[5]	1.03	0.13[5]	0.64
ion complexes[22]	anion binding	40	14.7	23	aug-cc-pVDZ	*tight*	*0.35*[22]	*1.55*	*0.10*[22]	*0.24*[†]
AC12[23]	carbene spin-states	12	15.6	23	cc-pVTZ	default	0.79[20]	0.92	0.24[11]	0.45
S66[24]	interactions	66	19.9	34	haug-cc-pVTZ	default	0.27[25]	1.00	0.16[25]	0.58
S66x8[26]	dimer dissociation	528	19.9	34	haug-cc-pVTZ	*tight*	*0.10*[13]	*0.65*	*0.05*[13]	*0.22*[†]
Ru-complexes[27]	TM reaction & barrier	180	25.2	41	def2-TZVPP	default	1.94[27]	6.65	0.36[27]	1.11[†]
ACONF12[28]	alkene conformation	12	38	38	aug-cc-pVTZ	default	0.24[14]	0.31	0.31[14]	0.39[†]
CEMS26[2]	react., interact., conf.	12	39	63	T-ζ & Q-ζ	default	0.74[5]	1.60	0.34[5]	1.01
C_{40} fullerenes[29]	isomerization	28	40	40	6-31G(d)	default	5.07[27]	11.7	0.86[29]	1.79[†]
MOBH35[30]	TM reaction & barrier	81[c]	41.6	65	def2-SVP	default	0.86[31]	3.86	0.13[31]	0.54[†]
polypyrrol[32]	reaction & barrier[b]	18	57.9	67	cc-pVDZ	*tight*	*1.02*[32]	*3.30*	*0.49*[32]	*1.71*[†]

[a] Obtained with an early, 2017 version of LNO-CCSD(T) with the tighter settings in Ref. 8 and the 2013 version of DLPNO-CCSD(T_0) with *TightPNO* settings.[33]

[b] Extended π-systems with including a few borderline multireference examples.

[c] Reactions 17–20 and 24–25 were omitted due to their size, and 8–9 were recommended to be omitted due to their multireference character in Ref. 31. The MAX local errors are larger for complexes 8 and 9, namely 2.41 kcal/mol for LNO-CCSD(T) and 14.96 kcal/mol for DLPNO-CCSD(T_1).

The NWH reaction energy benchmarks against DF-CCSD(T) are given in Fig. S3, as they represent similar trends to the S66 and CEMS26 examples in Fig. 9 of the main text (see Sect. 3.1). In brief, monotonic convergence can be observed for the statistical error measures with *NormalPNO* DLPNO-CCSD(T_1) being between *Loose* and *Normal* LNO-CCSD(T) and *TightPNO* DLPNO-CCSD(T_1) being between *Normal* and *Tight* LNO-CCSD(T). The default MAD errors of 0.13 kcal/mol for *Normal* LNO-CCSD(T) and 0.31 kcal/mol for *NormalPNO* DLPNO-CCSD(T_1) are already good.
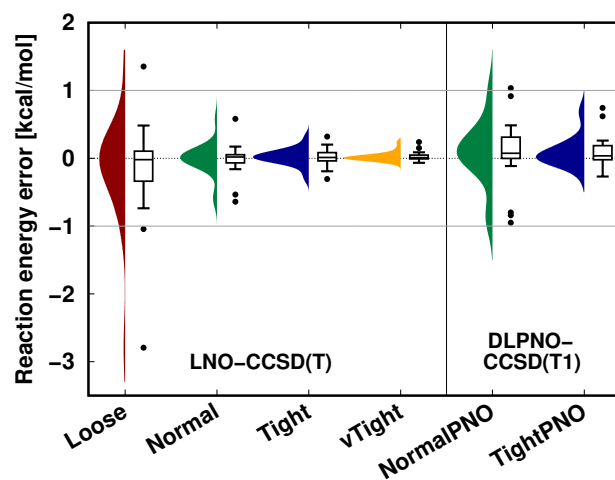
Figure S3: LNO-CCSD(T) (left) and DLPNO-CCSD(T_1) (right) reaction energy deviations against the DF-CCSD(T) reference in the cc-pVTZ basis set[5] for the NWH compilation.[21] The notation explanation and data source are given in the caption of Fig. 9 of the main text.

S6 Correlation energy benchmarks

The quality of the local CCSD(T) correlation energies are assessed for the $(AcOH)_2$ dimerization, octamethylcyclobutane (OMCB) formation reaction, and the halocyclization TS (Tables S2–S4). Here, reference DF-CCSD(T) energies are available for the smaller species, except for the halocyclization TS trimer. The purpose of the there examples is to illustrate how to assess the convergence of the correlation energies and the level of potential local error compensation upon forming energy differences. The first two examples show how this analysis works with the advantage of having the exact DF-CCSD(T) result, while the halocyclization TS is a real-life case illustrating what can be learned when the DF-CCSD(T) result is unavailable.

Table S2: Relative LNO-CCSD(T) and DLPNO-CCSD(T_1) local correlation energy errors [in %] with respect to the DF-CCSD(T)/haug-cc-pVTZ reference for the $(AcOH)_2$ dimer and the corresponding AcOH monomer of the S66 set,[24] supporting the dimerization energy convergence plot in Fig. 5 of the main text. (The two AcOH monomers are not identical, but their results agree for the presented number of digits.)

Threshold	$(AcOH)_2$ [%]	AcOH [%]	Compensated error [%]	[kcal/mol]
	LNO-CCSD(T)			
Loose	-0,134	-0,075	-0,058	0,64
Normal	-0,087	-0,054	-0,033	0,36
Tight	-0,034	-0,018	-0,015	0,17
veryTight	-0,007	-0,004	-0,004	0,04
L-N	-0,064	-0,044	-0,020	0,21
N-T	-0,007	0,000	-0,007	0,08
T-vT	0,006	0,003	0,002	-0,03
	DLPNO-CCSD(T_1)			
NormalPNO	-0,253	-0,169	-0,084	0,92
TightPNO	-0,074	-0,050	-0,024	0,26
VeryTightPNO	-0,035	-0,021	-0,014	0,15

Inspecting the first two columns of Table S2 and S3, the relative local CCSD(T) correlation energy errors converge monotonically for both the LNO and DLPNO results (maybe except for the *Loose* LNO case of OMCB). Especially the *veryTight* and the LAF extrapolated LNO-CCSD(T) results reach the 0.01% local error (or 99.99% accuracy), while *Very-*

TightPNO local errors in the 0.02-0.06% range are also reliable.

It is constructive to inspect the level of correlation error compensation as collected in the last two columns of Table S2 and S3 in percents and kcal/mol, respectively. Here, we take the correlation energy weighted average of the correlation energy errors at the two terms of the energy difference formation [e.g., separately for the dimer and monomers, or for the reactant(s) and product(s)]. For example, the resulting "Compensated error" measure is the same as the difference of the OMCB and 2,3-dimethylbut-2-ene (DMBE) relative errors, but, for the halocyclization reaction in Table S4, the reactant side is weighted according to the correlation energies of the two reactants and the catalyst. Consequently, the "Compensated error" in Tables S2–S4 is practically the local correlation error in the interaction and reaction energies of the $(AcOH)_2$ and OMCB examples (due to the two almost identical monomers and reactants), and it closely approximates the energy difference error if the relative errors of different species are weighted together (like for the halocyclization example).

Table S3: Relative LNO-CCSD(T) and DLPNO-CCSD(T_1) local correlation energy errors [in %] with respect to the DF-CCSD(T)/cc-pVTZ reference for the OMCB product and the corresponding 2,3-dimethylbut-2-ene (DMBE) reactant of the NWH set,[21] supporting the dimerization reaction energy convergence plot in Fig. 5 of the main text.

Threshold	OMCB [%]	DMBE [%]	Compensated error [%]	[kcal/mol]
		LNO-CCSD(T)		
Loose	0,030	-0,042	0,072	-1,06
Normal	-0,022	-0,020	-0,002	0,02
Tight	-0,026	-0,013	-0,013	0,19
veryTight	-0,017	-0,007	-0,010	0,15
L-N	-0,048	-0,009	-0,038	0,56
N-T	-0,028	-0,009	-0,019	0,27
T-vT	-0,012	-0,003	-0,009	0,13
		DLPNO-CCSD(T_1)		
NormalPNO	-0,199	-0,140	-0,060	0,88
TightPNO	-0,092	-0,051	-0,041	0,61
VeryTightPNO	-0,057	-0,030	-0,027	0,40

When comparing the "Compensated error" with the largest relative errors in the rows corresponding to a given local correlation setting for the individual species the LNO and

DLPNO errors are cut by a factor of ca. 2 and 2–3, respectively, for all three examples. This is in accord with our expectations, as these are examples where sizable local error compensation cannot occur. Nevertheless, while the similarly named DLPNO settings yield larger correlation energy errors than the corresponding LNO settings, their somewhat better error compensation leads to comparable *NormalPNO* DLPNO-CCSD(T$_1$) and *Loose* LNO-CCSD(T), or *TightPNO* DLPNO-CCSD(T$_1$) and *Normal* LNO-CCSD(T), or *VeryTightPNO* DLPNO-CCSD(T$_1$) and *Tight* LNO-CCSD(T) compensated errors.

These convergence trends look practically the same for the (AcOH)$_2$ dimerization and OMCB reaction with respect to two references: DF-CCSD(T) or local CCSD(T) converged to the hundredths of a percent or better errors. The benefit of the "Compensated error" measure is that it connects the convergence of the individual correlation energies and of the energy differences. In addition, the "Compensated error" can be computed also from the best available local CCSD(T) result, even if the exact DF-CCSD(T) is too costly. For the halocyclization barrier, we can employ vT–vvT LAF extrapolated LNO-CCSD(T) as a reference, but often T–vT or *veryTight* LNO-CCSD(T) can be similarly suitable for such an analysis. For example, the errors of vT–vvT LNO-CCSD(T) can be verified to be in the 0.002–0.005% range against DF-CCSD(T) for the three smaller species on the reactant side (see first raw of Table S4).

Taking this 0.002–0.005% uncertainty in the errors of Table S4 compared to vT–vvT LNO-CCSD(T), the convergence trends are similar to the smaller (AcOH)$_2$ and OMCB examples in terms of the rate of convergence and error compensation. Namely, the *Normal, Tight, vTight,* and *vvTight* LNO-CCSD(T) correlation energies show -0.050%, -0.024%, -0.008%, and -0.0027% relative deviations for the most complicated, TS structure. Compared to the same reference *NormalPNO, TightPNO*, and *VeryTightPNO* DLPNO-CCSD(T$_1$) correlation energies differ by -0.355%, -0.144%, and -0.115%, respectively. However, an important difference is that the halocyclization TS correlation energy is ca. 3960 kcal/mol. Thus even the 0.03–0.04% compensated errors of *Normal LNO-CCSD(T)* or *VeryTightPNO*

Table S4: Relative LNO-CCSD(T) and DLPNO-CCSD(T_1) local correlation energy deviations [in %] with respect to the vT–vvT LAF extrapolated LNO-CCSD(T)/aug-cc-pVTZ reference for species contributing to the halocyclization barrier height in Fig. 6 of the main text.

Thresholds	Ph-pent-ac [%]	DCDMH [%]	QUI [%]	TS [%]	Compensated error [%]	[kcal/mol]
			LNO-CCSD(T)			
vT–vvT vs DF-CCSD(T)	0,002	-0,005	0,002	-	-	-
Normal	-0,004	-0,065	0,027	-0,050	-0,032	1,27
Tight	0,006	-0,034	0,011	-0,024	-0,017	0,68
veryTight	0,006	-0,012	0,005	-0,008	-0,007	0,30
veryveryTight	0,002	-0,004	0,002	-0,003	-0,002	0,10
N–T	0,010	-0,018	0,002	-0,011	-0,010	0,38
T–vT	0,007	-0,002	0,003	-0,00004	-0,003	0,11
			DLPNO-CCSD(T_1)			
NormalPNO	-0,228	-0,299	-0,187	-0,355	-0,112	4,80
TightPNO	-0,085	-0,120	-0,077	-0,144	-0,048	2,05
VeryTightPNO	-0,052	-0,058	-0,043	-0,088	-0,036	1,55

DLPNO-CCSD(T_1) indicate about 1.3–1.6 kcal/mol respective error in their barrier heights. In other words, this example underlines the importance of accurate correlation energies when the local error compensation is small. For example, even the ca. 0.11% *NormalPNO* DLPNO-CCSD(T_1) compensated error points to 4–5 kcal/mol barrier height error.

S7   Additional systematic convergence examples

Here, we collect additional examples for systematic convergence with respect to both the local approximations and basis set, extending Sect. 3 of the main text.

Expanding first on the brief analysis of the acetic acid dimer interaction energies in Sect. 3.2 of the main text, Fig. S4 shows CBS(T,Q) and CBS(Q,5) CCSD(T) results within 0.07 kcal/mol from each other, indicating excellent basis set convergence close to the CBS limit. The *Loose–vTight* LNO-CCSD(T) energies also converge convincingly to the conventional CCSD(T) results (horizontal lines of matching color). While the *Loose* LNO-CCSD(T) errors of around 0.5–0.7 kcal/mol are not sufficient for quantitative purposes, the largest *Nor-*

mal, Tight, and *vTight* LNO errors for all five basis set levels reliably improve as ca. 0.4, 0.25, and 0.04 kcal/mol, respectively.
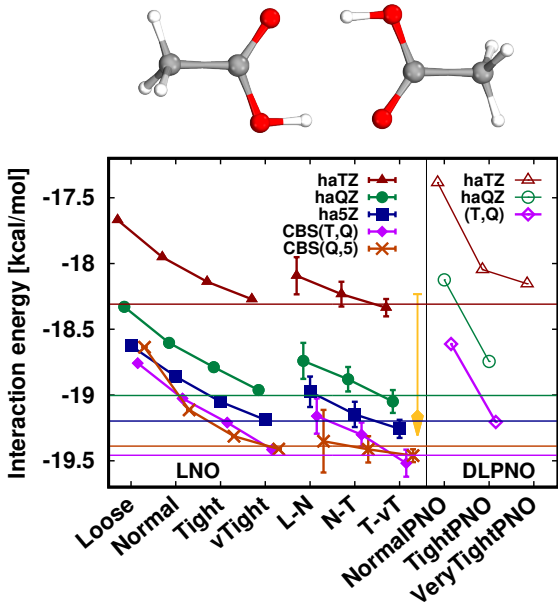

Figure S4: Interaction energy of the acetic acid dimer of the S66 compilation[24] using Counterpoise correction. The plot show LNO-CCSD(T) (left), LAF extrapolated LNO-CCSD(T) according to Eq. 5 (middle) and DLPNO-CCSD(T$_1$) (right) results compared to the horizontal lines corresponding to the conventional CCSD(T) results. The *Normal* LNO-CCSD(T)/ΔCBS(T,Q) basis set correction to *Normal–Tight* LNO-CCSD(T)/haTZ in the composite $E_{\mathrm{LAF}\ \mathrm{CCSD(T)}}^{\mathrm{CBS(X,X+1),X}}$ approach of Eq. 7 is depicted as an orange vertical arrow.

The next three examples (Figs. S5–S7) have representative systems size (ca. 60–90 atoms) and show relatively fast convergence toward the conventional CCSD(T)/CBS result. The reaction energy corresponding to the formation of androstendione from its precursor is a relatively simple organic reaction (Fig. S5).[5] For the second example, the interaction energy for a phenylalanine residue trimer (formed from a monomer and a dimer as defined in the L7 set[34]) is taken based on our data from Ref. 16. For the third example, the difference of two barrier heights are studied for the Michael-addition reaction discussed also in Sect. 3.3 of the main text. The two transition states lead to different stereoisomers of the product and thus play a crucial role in exploring the stereochemical details of this reaction mechanism.[35]

These three examples, while having a considerable system size, exhibit relatively fast convergence, especially with the LNO approximations. Already the N-T uncertainty estimates
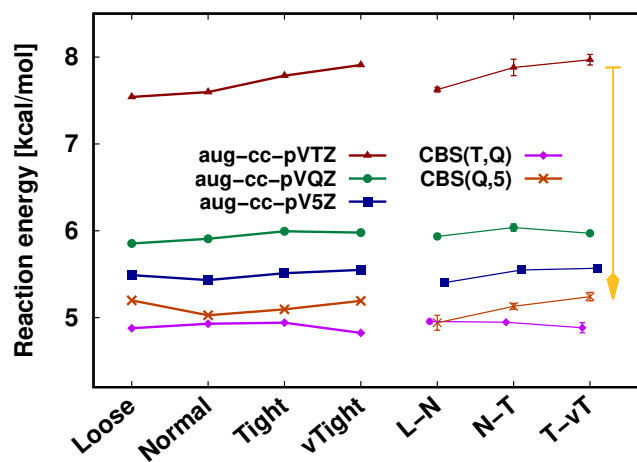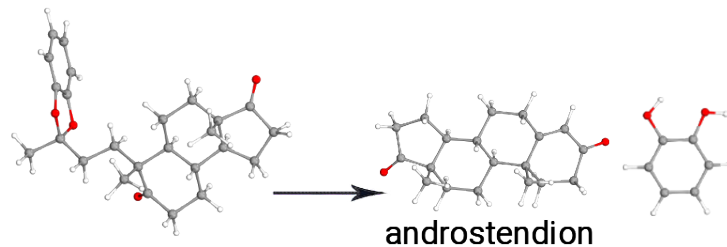
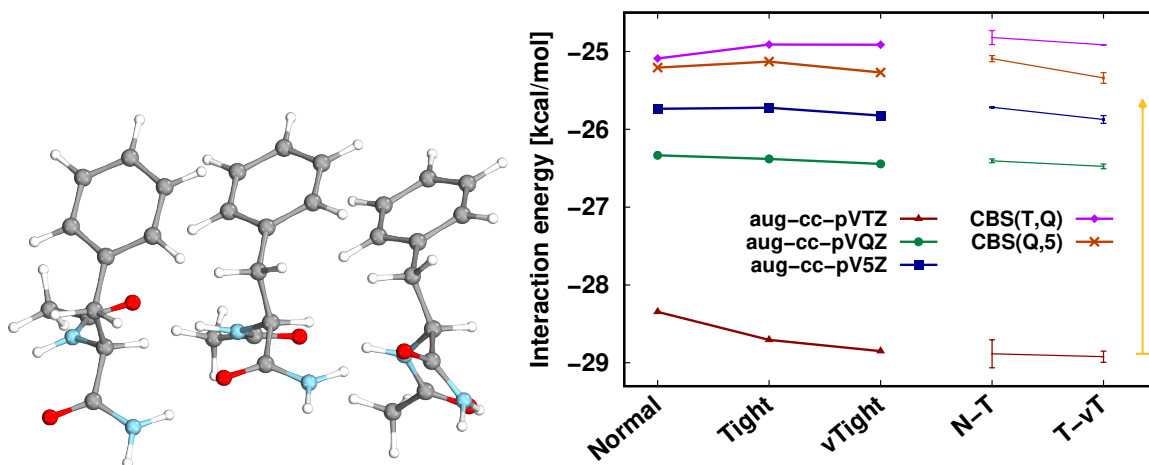Figure S5: Reaction energy for the formation of androstendione from its precursor with the LNO-CCSD(T) method.[5]

Figure S6: Interaction energy of the phenylalanine residue trimer (from the L7 set[34]) with the LNO-CCSD(T) method.[16]

are below 0.1 kcal/mol (with the only exception of ±0.18 kcal/mol for the aug-cc-pVTZ result of Fig. S6), and even the *Loose* or L-N are well within chemical accuracy. For these cases in Figs S5–S7, CBS(T,Q) and when available even CBS(D,T) basis set levels are also
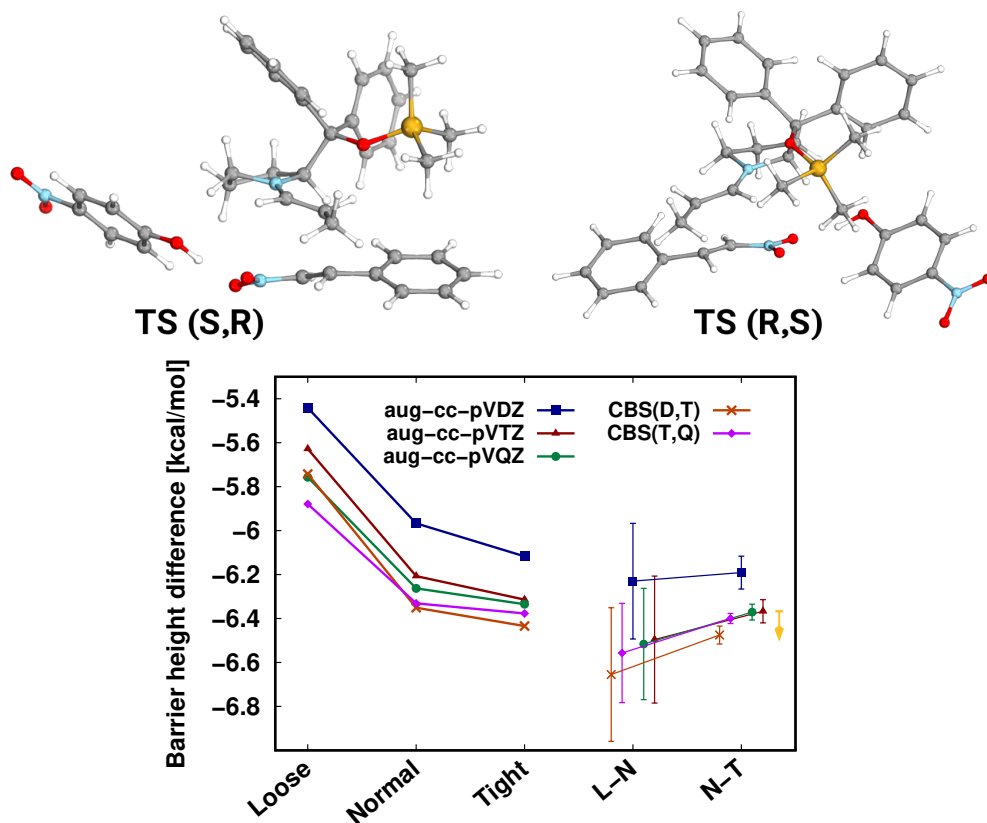
highly accurate.

Figure S7: Barrier height differences between two transition state structures taken from the stereoselectivity study of Ref. 35.

The fast convergence can be attributed to the relatively high level of similarity on the two sides of the energy differences, which is a frequently occurring scenario. For example, the reactant and product side of the reaction forming androstendione are relatively similar. A minor difficulty is cased by the intermolecular BSSE between the atoms of the two product molecules as shown by an about 3 kcal/mol basis set error at the aug-cc-pVTZ level. While the interaction energy is considerable for the phenylalanine residue trimer, the interacting surface is not as large and the individual interaction components (mostly dispersion and H-bonding) are not very problematic either for local approximations. Here, excellent basis set convergence is also found even without Counterpoise corrections, while the Counterpoise corrected interaction energies show only ca. 0.1 kcal/mol basis set error

already at the aug-cc-pVTZ level.[16] The largest error compensation can be expected for the barrier height difference example of Fig. S7, where the same interactions are found in both sides with a different spatial orientation. Here, already the *Normal* LNO-CCSD(T)/aug-cc-pVTZ results are converged to almost 0.1 kcal/mol, and for most purposes even *Normal* LNO-CCSD(T)/aug-cc-pVDZ is sufficient.

In contrast to the average examples, we also show an interaction and reaction energy example which are considerably more complicated than the average applications (Figs. S8 and S9). First, the coronene dimer (Fig. S8) is extensively studied also by multiple high-quality wave function methods, including LNO-, DLPNO-, PNO-LCCSD(T), FN-DMC, etc., but here we focus on the convergence of the local approximations and refer to its extensive literature.[4,16,36–41]
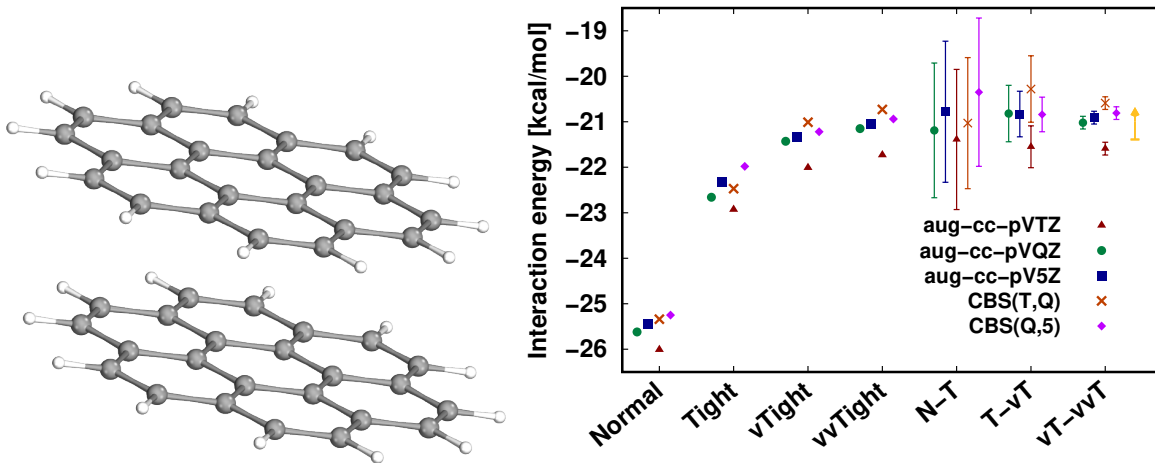

Figure S8: Interaction energy of the coronene dimer with the LNO-CCSD(T) method using Counterpoise corrections.[16] Some results are slightly shifted along the x-axis to increase visibility.

The convergence of the LNO approximations is again reliable for the coronene dimer interaction energies of Fig. S8. The main difference compared to the other examples is in the magnitude of the local correlation errors. In this case, *Tight* LNO-CCSD(T) settings are needed to reach the edge of chemical accuracy. However, the systematic convergence and the LAF extrapolation remain robust, as shown by the few tenths of a kcal/mol agreement between the *veryveryTight*, N–T, T–vT, vT–vvT LNO-CCSD(T) results. Moreover, the

LNO error bars reliably decrease and envelope the LAF limit, reaching only about ±0.15 kcal/mol uncertainty at the vT–vvT LNO-CCSD(T) level. The coronene dimer is challenging for other local methods, too. For example, using diffuse basis sets leads to severe basis set redundancy issues, which cannot be treated with any other local CC method, and can only be circumvented in the LNO-CCSD(T) implementation. Thus, most previous DLPNO-CCSD(T) computations had to rely on relatively small, double- or triple-ζ basis sets, often without diffuse basis functions, combined with low-level (mostly MP2) basis set corrections. However, the interaction energy error of MP2 with respect to CCSD(T) is close to 100% in this case, which discourages the use of MP2-based basis set incompleteness corrections. The significant, about 2.2 kcal/mol step between the *TightPNO* and *VeryTightPNO* results reported in Ref. 41 also indicates the challenges of converging the DLPNO or, in fact, any local correlation results. While the BSSE is above 10 kcal/mol at the triple-ζ level,[16] Counterpoise corrections and CBS extrapolation lead to reliable basis set convergence for LNO-CCSD(T).
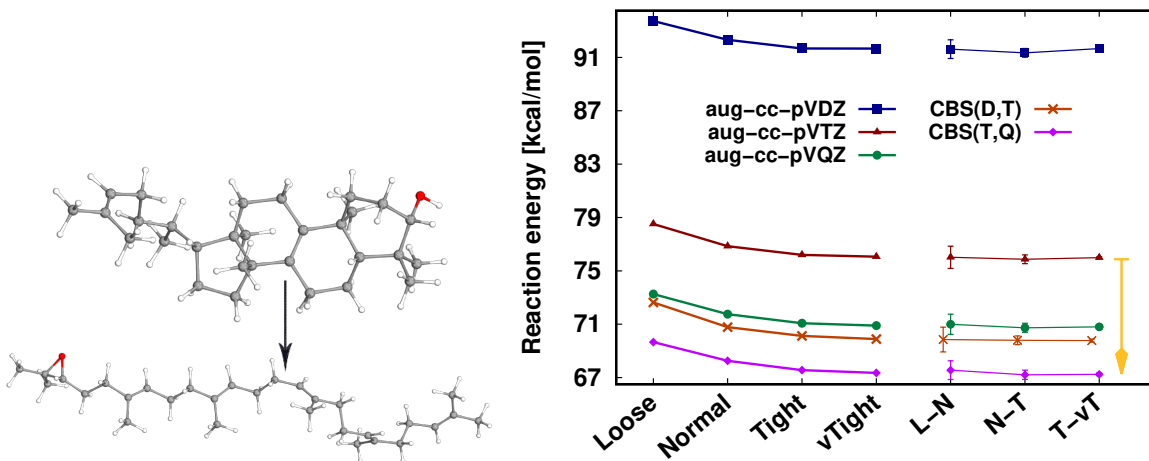

Figure S9: Reaction energy of lanosterol to (S)-2,3-oxidosqualene (ISOL4)[42] with the LNO-CCSD(T) method.[5]

The second challenging case is the fourth reaction of the isomerization test set (ISOL4) of Grimme and co-workers (Fig. S9).[42] Here, the two intermediate steps in the biosynthesis of cholesterol, lanosterol [ISOL4 educt] and (S)-2,3-oxidosqualene [ISOL4 product] are

markedly different, separated by many elementary steps of the net reaction. Therefore one cannot rely on any error compensation between the educt and product. First, the basis set incompleteness errors at the aug-cc-pVDZ and aug-cc-pVTZ levels are about 24 and 8-9 kcal/mol, respectively, with respect to the CBS(T,Q) reaction energies.[5] Compared to that, the LNO uncertainty convergence is acceptable, namely 0.7-0.8, 0.3-0.4, and at most 0.1 kcal/mol error bars are assigned to the L-N, N-T, and T-vT LAF extrapolated LNO-CCSD(T) results.

S8   Correlation energy error statistics

Here, we collect the correlation energy error statistics to provide more background to the corresponding energy difference analysis of Sect. 4 in the main text. The available information includes in Table S5 the mostly default and partly tight LNO and DLPNO correlation energy errors for 10 compilations (of the 14 sets in Table 4 of the main text). Additionally, the convergence of the LNO and DLPNO relative correlation energy errors with respect to the local threshold sets are shown for the NWH,[21] S66,[24] and CEMS26[2] compilations in Fig. S10, supplementing the corresponding energy difference convergence statistics in Figs. S3, and 9.

In brief, the average (maximum) LNO correlation energy errors in Table S5 are mostly below 0.03-0.07% (0.1%) with only a handful of exceptions, as noted in Sect. 4 of the main text. Compared to that, the relative DLPNO-CCSD(T_1) correlation energy errors in Table S5 are in most cases 3–5 times larger than that of LNO-CCSD(T). However, this difference between the LNO and DLPNO performance is notably larger than the corresponding energy difference deviations in Table 4 of the main text. A better understanding of this comparison is offered by looking also at the distribution of the relative correlation energy errors of Fig. S10. There, we find a similar width and shape for the *NormalPNO* DLPNO-CCSD(T_1) with *Loose* or *Normal* LNO-CCSD(T) and for *TightPNO* DLPNO-CCSD(T_1) with *Normal* and *Tight* LNO-CCSD(T), aside from a shift along the vertical axis. Thus, taking into

account a possible compensation of some of the DLPNO-CCSD(T_1) correlation energy errors responsible for the shift with respect to the LNO-CCSD(T) results provides an explanation that is more consistent with the experience found for the energy difference errors in the main text.

Table S5: Summary of local CCSD(T) benchmarks in the literature for correlation energies corresponding to the energy difference benchmarks of Table 4 of the main text. Mean absolute error (MAE) and maximum errors [in %] relative to canonical CCSD(T) for the LNO-CCSD(T) and DLPNO-CCSD(T_1) methods are collected in the last columns corresponding to their default or tight (italicized) settings. Results in rows labeled with [†] symbols were evaluated independently from LNO and DLPNO method developers.

test set	property	entries	No. of atoms		threshold	DLPNO error		LNO error		
			AVG	MAX		MAE	MAX	MAE	MAX	
RSE30 [19]	radical reactions	62	9.3	13	default	0.148 [20]	0.313	0.029 [11]	0.081	
IP21 [10]	ionization	42	9.8	17	default	0.183 [20]	0.627	0.047 [11]	0.109	
NWH [21]	reactions	47	13.5	36	default	0.160 [5]	0.308	0.024 [5]	0.092	
AC12 [23]	carbene spin-states	24	15.6	23	default	0.296 [20]	0.406	0.043 [11]	0.084	
S66 [24]	interactions	198	19.9	34	default	0.141 [5]	0.302	0.029 [5]	0.094	
S66x8 [13]	dimer dissociation	660	19.9	34	tight	*0.034* [31]	*0.097*	*0.017* [31]	*0.045*	[†]
ACONF [28]	alkene conformation	13	38	38	default	0.149 [14]	0.164	0.029 [14]	0.049	[†]
CEMS26 [2]	reac., inter., conf.	26	39	63	default	0.236 [5]	0.430	0.067 [5]	0.145	
MOBH35 [30]	TM reaction barriers	81[a]	41.6	65	default	0.542 [31]	1.373	0.026 [31]	0.074	[†]
polypyrrol [32]	reaction & barrier[b]	21	57.9	67	tight	*0.181* [32]	*0.241*	*0.063* [32]	*0.089*	[†]

[a] Reactions 17–20 and 24–25 were omitted due to their size and 8–9 were recommended to be omitted due to their multireference character. [31]

[b] Extended π-systems with multiple borderline multireference examples.
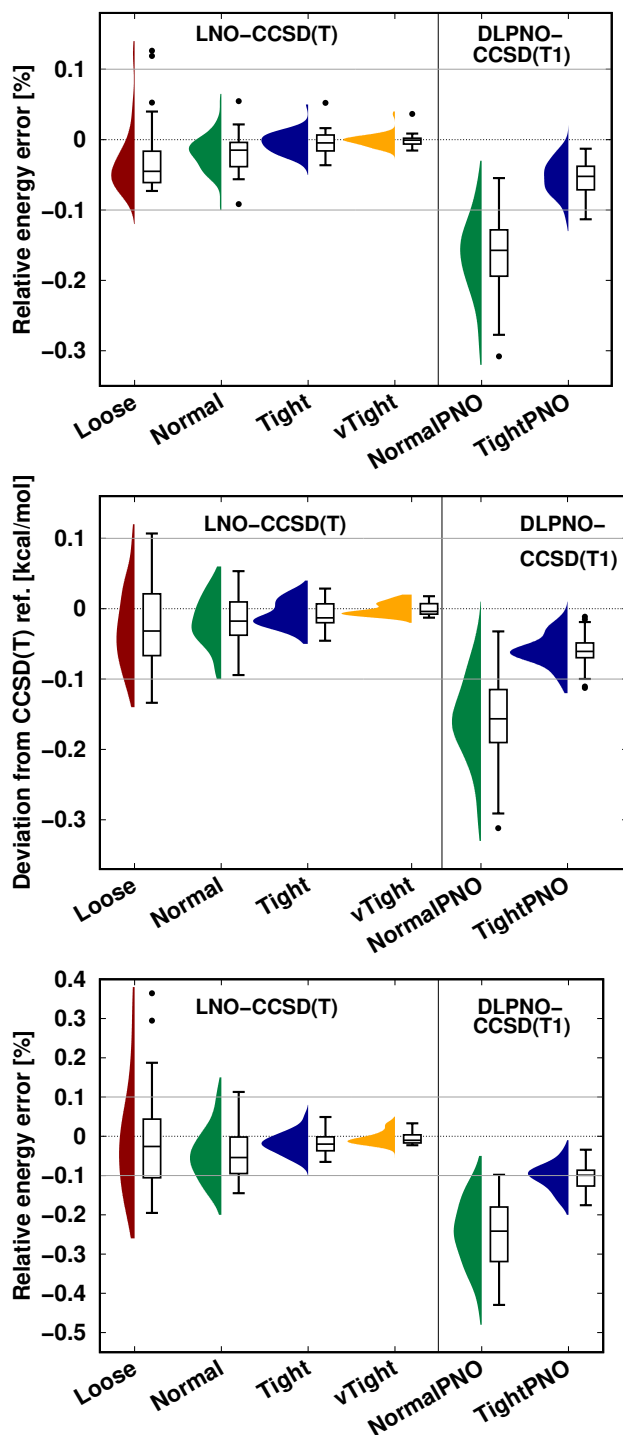
Figure S10: LNO-CCSD(T) (left sides) and DLPNO-CCSD(T_1) (right sides) correlation energy deviations with respect to the DF-CCSD(T) reference. Top panel: NWH compilation[21] (cc-pVTZ basis set).[5] Middle panel: dimers of the S66 compilation[24] (haug-cc-pVTZ basis set).[25] Bottom panel: CEMS26 compilation.[5] Source of data: Tables 2 and S1 of Ref. 5 and Ref. 25.

S9 Additional computational requirement measurements

Wall-time measurement for the Michael-addition TS structure are reported in Fig. S11 (analogously to the case of the halocyclization TS in Fig. 10 and corresponding discussion in the main text.)
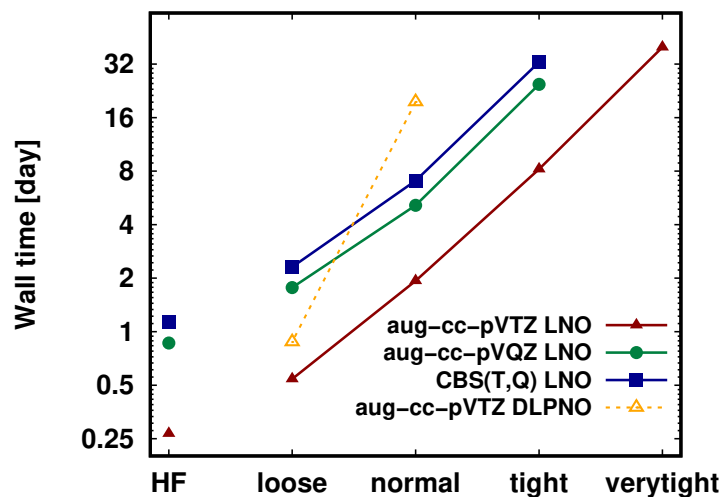

Figure S11: DF-HF, LNO-CCSD(T) (solid lines) and DLPNO-CCSD(T$_1$) (dashed) wall time measurements [in days] on 6 cores for the 90-atom TS of the Michael-addition reaction in Fig. 7 of the main text with various basis set choices. The time plotted for the CBS(T,Q) result is the sum of the aug-cc-pVTZ and aug-cc-pVQZ wall times.

Moreover, we show on the specific example of the halocyclization TS, how the errors depend on the computational requirements. For this purpose, Fig. S12 combines the wall time measurements from Fig. 10 of the main text with the energy errors obtained from the convergence test of Fig. 6 from the main text.
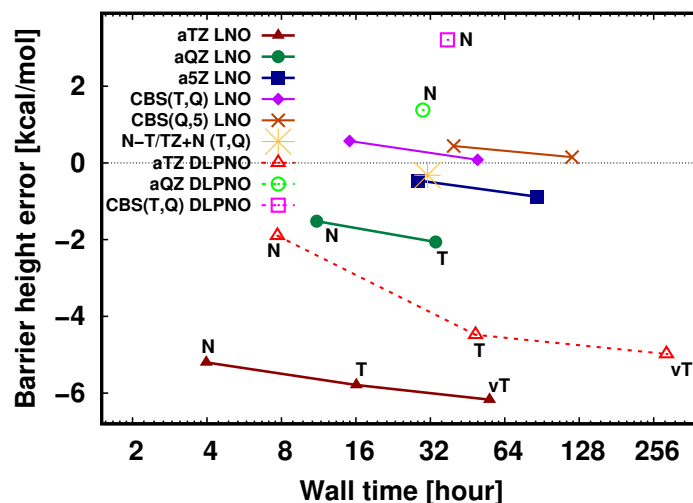
Figure S12: Barrier height errors [in kcal/mol] for the halocyclization reaction (Fig. 6 of the main text) plotted as a function of the wall time requirement (16 cores) reported in Fig. **??** of the main text. The N, T, vT, as well as 'N-T/TZ+N (T,Q)' shorthands label the *Normal(PNO)*, *Tight(PNO)*, *veryTight(PNO)* settings and the $E_{\text{N-T LNO-CCSD(T)}}^{\text{CBS(T,Q),T}}$ composite method.

S10   Computational details

The LNO-CCSD(T) computations were performed with the MRCC package using multiple releases by us and by independent users over the years.[43,44] Similarly, multiple versions, namely 4.0, 4.1, 4.2, and 5.0 of the ORCA package were employed for the DLPNO-CCSD(T) computations.[45] The appropriate MRCC and ORCA code versions can be found in the original cited publications. However, for both the LNO and DLPNO methods the latest method and code versions are recommended due to their ongoing developments. The open-shell LNO-CCSD(T) computations are made with the development version of MRCC,[43,44] which will be made available in a forthcoming release. Both MRCC and ORCA are free for academic purposes and they both facilitate commercial use. MRCC is also open-source for academic use.

A typical LNO-CCSD(T) input file looks as follows:

```
calc=LNO-CCSD(T)
basis=aug-cc-pVTZ
mem=25gb
localcc=2021
lcorthr=tight
geom=xyz
2

H 0.00000000000000 0.00000000000000 -0.3715911499
H 0.00000000000000 0.00000000000000 0.3715911499
```

The wall-time measurements were performed via shared-memory OpenMP parallelization for LNO-CCSD(T) in MRCC and replicated-memory MPI parallelization for DLPNO-CCSD(T_1) in ORCA. For the 63-atom halocyclization TS in Fig. 10 of the main text we used 16 cores of a 64-core 2.45 GHz AMD EPYC 7763 CPU for both LNO-CCSD(T) and DLPNO-CCSD(T_1). The optimal memory allocations were 5, 10, 14, and 20 GBs for the *Loose, Normal, Tight,* and *veryTight* LNO-CCSD(T)/aug-cc-pVTZ computations in Fig. 10. Since the memory demand of DLPNO-CCSD(T_1)/aug-cc-pVTZ computations is higher, the entire memory of the 128-core dual-CPU node was used for the 16-core DLPNO-CCSD(T_1)

computations. That is, for each of the 16 MPI tasks 13 GB memory was allocated, total-ing 16*13=208 GB memory use for the DLPNO-CCSD(T_1) computations. For the 90-atom Michael-addition TS in Fig. S11 of the main text we used a 6-core 3.5 GHz Intel Xeon E5-1650 v2 CPU node with a local hard drive for both LNO-CCSD(T) and DLPNO-CCSD(T_1). The optimal memory allocations were 16, 26, 36, and 43 GB for the *Loose*, *Normal*, *Tight*, and *veryTight* LNO-CCSD(T)/aug-cc-pVTZ computations. For the DLPNO-CCSD(T_1) compu-tation the entire node memory (126 GB) was enabled, that is 6 tasks times 21 GB/task memory was used.

S11   CBS extrapolation

The CBS limit of the HF and correlation energies is approached via standard two-point extrapolation techniques but any other extrapolation formula developed for conventional methods can also be adopted. The compact notation of $\mathrm{CBS}(X, X+1)$ is employed to denote extrapolation using the X-ζ and $(X + 1)$-ζ bases. For instance, extrapolated results based on the aug-cc-pVTZ and aug-cc-pVQZ sets is labeled by CBS(T,Q). For the extrapolation of HF energies the two-point formula suggested by Karton and Martin[46] is used:

$$E_{X(X-1)}^{\mathrm{HF}} = E_X^{\mathrm{HF}} + \frac{(E_X^{\mathrm{HF}} - E_{X-1}^{\mathrm{HF}})(X + 1)}{X \exp\left(\gamma(\sqrt{X} - \sqrt{X-1})\right)} \,, \tag{S7}$$

where E_X^{HF} is the HF energy obtained with the X-ζ basis set and γ is 6.57 or 9.03 for $X = 4$ or $X = 5$, respectively.[46] Correlation energies are extrapolated using the formula introduced by Helgaker *et al.*[47] as

$$E_{X(X+1)}^{\mathrm{corr}} = \frac{X^3 E_X^{\mathrm{corr}} - (X + 1)^3 E_{X+1}^{\mathrm{corr}}}{X^3 - (X + 1)^3} \,, \tag{S8}$$

with E_X^{corr} being the correlation energy with the X-ζ basis set. For smaller basis sets, e.g., for CBS(D,T) extrapolations, the exponents optimized by Neese and Valeev can be employed.[48]

References

(1) Kurashige, Y.; Yang, J.; Chan, G. K.-L.; Manby, F. R. *J. Chem. Phys.* **2012**, *136*, 124106.

(2) Nagy, P. R.; Samu, G.; Kállay, M. *J. Chem. Theory Comput.* **2018**, *14*, 4193.

(3) Guo, Y.; Riplinger, C.; Becker, U.; Liakos, D. G.; Minenkov, Y.; Cavallo, L.; Neese, F. *J. Chem. Phys.* **2018**, *148*, 011101.

(4) Ma, Q.; Werner, H.-J. *Wiley Interdiscip. Rev.: Comput. Mol. Sci.* **2018**, *8*, e1371.

(5) Nagy, P. R.; Kállay, M. *J. Chem. Theory Comput.* **2019**, *15*, 5275.

(6) Nagy, P. R.; Samu, G.; Kállay, M. *J. Chem. Theory Comput.* **2016**, *12*, 4897.

(7) Gyevi-Nagy, L.; Kállay, M.; Nagy, P. R. *J. Chem. Theory Comput.* **2020**, *16*, 366.

(8) Nagy, P. R.; Kállay, M. *J. Chem. Phys.* **2017**, *146*, 214106.

(9) Neese, F. *J. Am. Chem. Soc.* **2006**, *128*, 10213.

(10) Szabó, P. B.; Csóka, J.; Kállay, M.; Nagy, P. R. *J. Chem. Theory Comput.* **2021**, *17*, 2886.

(11) Szabó, P. B.; Csóka, J.; Kállay, M.; Nagy, P. R. *J. Chem. Theory Comput.* **2023**, *19*, 8166.

(12) Altun, A.; Neese, F.; Bistoni, G. *J. Chem. Theory Comput.* **2020**, *16*, 6142.

(13) Santra, G.; Semidalas, E.; Mehta, N.; Karton, A.; Martin, J. M. L. *Phys. Chem. Chem. Phys.* **2022**, *24*, 25555.

(14) Santra, G.; Martin, J. M. *J. Phys. Chem. A* **2022**, *126*, 9375.

(15) Liakos, D. G.; Neese, F. *J. Phys. Chem. A* **2012**, *116*, 4801.

(16) Al-Hamdani, Y. S.; Nagy, P. R.; Barton, D.; Kállay, M.; Brandenburg, J. G.; Tkatchenko, A. *Nat. Commun.* **2021**, *12*, 3927.

(17) Shi, B.; Zen, A.; Kapil, V.; Nagy, P. R.; Grüneis, A.; Michaelides, A. *J. Am. Chem. Soc.* **2023**, *145*, 25372.

(18) Paulechka, E.; Kazakov, A. *J. Chem. Theory Comput.* **2018**, *14*, 5920.

(19) Ma, Q.; Werner, H.-J. *J. Chem. Theory Comput.* **2020**, *16*, 3135.

(20) Szabó, P. B.; Csóka, J.; Kállay, M.; Nagy, P. R. **2024**,

(21) Neese, F.; Wennmohs, F.; Hansen, A. *J. Chem. Phys.* **2009**, *130*, 114108.

(22) Sandler, I.; Sharma, S.; Chan, B.; Ho, J. *J. Phys. Chem. A* **2021**, *125*, 9838.

(23) Ghafarian Shirazi, R.; Neese, F.; Pantazis, D. A. *J. Chem. Theory Comput.* **2018**, *14*, 4733.

(24) Řezáč, J.; Riley, K. E.; Hobza, P. *J. Chem. Theory Comput.* **2011**, *7*, 2427.

(25) Nagy, P. R.; Gyevi-Nagy, L.; Lőrincz, B. D.; Kállay, M. *Mol. Phys.* **2023**, *121*, e2109526.

(26) Řezáč, J.; Riley, K. E.; Hobza, P. *J. Chem. Theory Comput.* **2011**, *7*, 3466.

(27) Efremenko, I.; Martin, J. M. L. *J. Phys. Chem. A* **2021**, *125*, 8987.

(28) Ehlert, S.; Grimme, S.; Hansen, A. *J. Phys. Chem. A* **2022**, *126*, 3521.

(29) Karton, A.; Chan, B. *Comput. Theor. Chem.* **2022**, *1217*, 113874.

(30) Iron, M. A.; Janes, T. *J. Phys. Chem. A* **2019**, *123*, 3761.

(31) Semidalas, E.; Martin, J. M. L. *J. Chem. Theory Comput.* **2022**, *18*, 883.

(32) Sylvetsky, N.; Banerjee, A.; Alonso, M.; Martin, J. M. L. *J. Chem. Theory Comput.* **2020**, *16*, 3641.

(33) Riplinger, C.; Sandhoefer, B.; Hansen, A.; Neese, F. *J. Chem. Phys.* **2013**, *139*, 134101.

(34) Sedlak, R.; Janowski, T.; Pitoňák, M.; Řezáč, J.; Pulay, P.; Hobza, P. *J. Chem. Theory Comput.* **2013**, *9*, 3364.

(35) Földes, T.; Madarász, Á.; Révész, Á.; Dobi, Z.; Varga, S.; Hamza, A.; Nagy, P. R.; Pihko, P. M.; Pápai, I. *J. Am. Chem. Soc.* **2017**, *139*, 17052.

(36) Benali, A.; Shin, H.; Heinonen, O. *J. Chem. Phys.* **2020**, *153*, 194113.

(37) Ballesteros, F.; Dunivan, S.; Lao, K. U. *J. Chem. Phys.* **2021**, *154*, 154104.

(38) Christensen, A. S.; Elstner, M.; Cui, Q. *J. Chem. Phys.* **2015**, *143*, 084123.

(39) Carter-Fenk, K.; Lao, K. U.; Liu, K.-Y.; Herbert, J. M. *J. Phys. Chem. Lett.* **2019**, *10*, 2706.

(40) Calbo, J.; Ortí, E.; Sancho-García, J. C.; Aragó, J. *J. Chem. Theory Comput.* **2015**, *11*, 932.

(41) Pavošević, F.; Peng, C.; Pinski, P.; Riplinger, C.; Neese, F.; Valeev, E. F. *J. Chem. Phys.* **2017**, *146*, 174108.

(42) Huenerbein, R.; Schirmer, B.; Moellmann, J.; Grimme, S. *Phys. Chem. Chem. Phys.* **2010**, *12*, 6940.

(43) Kállay, M.; Nagy, P. R.; Mester, D.; Rolik, Z.; Samu, G.; Csontos, J.; Csóka, J.; Szabó, P. B.; Gyevi-Nagy, L.; Hégely, B.; Ladjánszki, I.; Szegedy, L.; Ladóczki, B.; Petrov, K.; Farkas, M.; Mezei, P. D.; Ganyecz, Á. *J. Chem. Phys.* **2020**, *152*, 074107.

(44) Kállay, M.; Nagy, P. R.; Mester, D.; Gyevi-Nagy, L.; Csóka, J.; Szabó, P. B.; Rolik, Z.; Samu, G.; Csontos, J.; Hégely, B.; Ganyecz, Á.; Ladjánszki, I.; Szegedy, L.; Ladóczki, B.; Petrov, K.; Farkas, M.; Mezei, P. D.; Horváth, R. A. Mrcc, *a quantum chemical program suite. See https://www.mrcc.hu/* **Accessed August 28, 2023**,

(45) Neese, F. *Wiley Interdiscip. Rev.: Comput. Mol. Sci.* **2017**, *8*, e1327.

(46) Karton, A.; Martin, J. M. L. *Theor. Chem. Acc.* **2006**, *115*, 330.

(47) Helgaker, T.; Klopper, W.; Koch, H.; Noga, J. *J. Chem. Phys.* **1997**, *106*, 9639.

(48) Neese, F.; Valeev, E. F. *J. Chem. Theory Comput.* **2011**, *7*, 33.